Effects of Codoping With Divalent Cations on Performance of YAG:Ce,C Scintillator

I. Gerasymov, S. Witkiewicz-Lukaszek, T. Zorenko, K. Bartosiewicz, Yu Zorenko, J. Winiecki, D. Kofanov, Ya Boyaryntseva, S. Tkachenko, P. Arhipov, E. Galenin, D. Kurtsev, O. Zelenskaya, V. Alekseev, K. Lebbou, and O. Sidletskiy

***Abstract*— Growth technologies of oxide crystals in W/Mo crucibles have been developed as a low-cost alternative to conventional processes involving Ir crucibles. Carbon-containing atmosphere needed to protect crucibles from oxidation leads to the introduction of carbon into the crystal lattice and creation of carbon-related defects, which affect the scintillation performance. Meanwhile, a search for fast scintillators for the new generation of positron-emission tomographs and high-energy physics experiments at colliders is under way. Codoping with divalent cations has become an efficient way to suppress long components of scintillation decay in Ce-doped scintillators. This work addresses $Y_3Al_5O_{12}$ (YAG) crystals codoped with carbon, cerium activator, and divalent cations. Optical and scintillation properties of YAG:Ce,C,A^{2+} crystals (A = Ca^{2+}, Mg^{2+}, Ba^{2+}, Sr^{2+}) are systematically studied. Among all the studied garnet compounds, YAG:Ce,C,Ca^{2+} crystals demonstrated the fastest scintillation decay times, which are promising for the mentioned applications. Mechanisms of scintillation process in the studied materials are discussed. The Ce^{3+}/Ca^{2+} ratio in YAG:Ce,C,Ca^{2+} was optimized to minimize slow components in scintillation decay.**

***Index Terms*— Codoping, crystal growth, scintillator, W crucible, yttrium aluminum garnet.**

Manuscript received 19 October 2022; revised 25 March 2023 and 22 April 2023; accepted 22 April 2023. Date of publication 25 April 2023; date of current version 18 July 2023. The work of I. Gerasymov, D. Kofanov, Ya Boyaryntseva, S. Tkachenko, P. Arhipov, E. Galenin, D. Kurtsev, O. Zelenskaya, V. Alekseev, and O. Sidletskiy was supported in part by the National Academy of Science of Ukraine Project "Carbon-2" under Grant 0122U002637 and in part by Ukrainian–French Project "Dnipro" under Grant 0122U200403 and Agreements M/36-2021 and M/44-2022. The work of T. Zorenko, K. Bartosiewicz, and Yu Zorenko was supported by Polish National Center of Science of Poland NCN projects under Grant 2018/31/B/ST8/03390 and Grant 2020/39/D/ST3/02711. The work of O. Sidletskiy was supported by the project "Centre of Excellence in nanophotonics, advanced materials and technologies based on crystal growth" (ENSEMBLE3) carried out within the International Research Agendas Program of the Foundation for Polish Science and Teaming for Excellence Project under Grant MAB/2020/14 and Grant 857543.

I. Gerasymov, D. Kofanov, Ya Boyaryntseva, S. Tkachenko, P. Arhipov, E. Galenin, D. Kurtsev, O. Zelenskaya, and V. Alekseev are with the Institute for Scintillation Materials NAS of Ukraine, 61072 Kharkiv, Ukraine.

S. Witkiewicz-Lukaszek, T. Zorenko, and K. Bartosiewicz are with the Institute of Physics, Kazimierz Wielki University, 85090 Bydgoszcz, Poland (e-mail: s-witkiewicz@wp.pl; tzorenko@ukw.edu.pl).

Yu Zorenko is with the Institute of Physics, Kazimierz Wielki University, 85090 Bydgoszcz, Poland, and also with the Oncology Center, Medical Physics Department, 85796 Bydgoszcz, Poland.

J. Winiecki is with the Oncology Center, Medical Physics Department, 85796 Bydgoszcz, Poland (e-mail: janusz@co.bydgoszcz.pl).

K. Lebbou is with the Institute Lumière Matière UMR 5306, Université Lyon, Université Claude Bernard Lyon 1, CNRS, 69100 Villeurbanne, France (e-mail: kheirreddine.lebbou@univ-lyon1.fr).

O. Sidletskiy is with the Institute for Scintillation Materials NAS of Ukraine, 61072 Kharkiv, Ukraine, and also with the Centre of Excellence ENSEMBLE3 Sp. z o. o., 01-919 Warsaw, Poland (e-mail: sidletskiy@isma.kharkov.ua).

Color versions of one or more figures in this article are available at https://doi.org/10.1109/TNS.2023.3270320.

Digital Object Identifier 10.1109/TNS.2023.3270320

I. Introduction

CODOPING with mono- or divalent cations is a common strategy for enhancing the performance of Ce^{3+}-doped scintillators. There are positive examples of the energy-resolution enhancement in $LaBr_3$:Ce,Sr [1], whereas scintillation decay acceleration and afterglow suppression were reported in Ce–Mg^{2+}- or Ce–Ca^{2+}-codoped complex oxides such as rare Earth orthosilicates (LSO), garnets ($Y_3Al_5O_{12}$ (YAG), LuAG, and GAGG) [2], [3], [4], [5], [6], and perovskites (YAP) [7]. Mg^{2+}-codoping of GAGG:Ce, the brightest oxide scintillator, was proposed for detectors at the upgraded Large Hadron Collider b (LHCb) calorimeter where a main decay time of up to 15 ns and a light yield of at least 15 000 phot/MeV are targeted [8].

However, providing a fast timing while keeping the light yield on a reasonable level is challenging. Introduction of mono- or divalent cations into trivalent cation sites creates an excessive negative charge that may be compensated by Ce^{3+} transfer into the tetravalent state, while the increased concentration of single Ce^{4+} centers provides a faster radiative de-excitation [3]. Meanwhile, Ce^{4+}–Mg^{2+} pairs with a lower barrier for thermal quenching from the $5d_1$ excited state of cerium at heavy Mg^{2+}-doping contribute to thermal quenching of Ce^{3+} scintillation yield [9]. Therefore, acceleration of the scintillation decay time in garnets at heavy Mg^{2+}-doping is achieved at the expense of light yield [8].

Recently, we have introduced the crystals of carbon-containing garnets, obtained as a result of crystal growth in carbon-containing atmosphere. Some enhancement of light yield with carbon doping was reported, while timing characteristics were similar [10] or slower [11] as compared to garnets obtained from Ir crucibles under conventional conditions of neutral atmosphere. In the same works, the light yield enhancement in YAG:Ce,C up to ca. 30 000 phot/MeV and LuAG:Ce,C and LuYAG:Ce up to ca. 27 000 phot/MeV was attributed to the creation of negatively charged carbon-containing defects, prevailing over intrinsic defects, such as oxygen vacancies or antisites responsible for intrinsic emission, and formation of trapping centers. They cause deterioration of scintillation

© 2023 The Authors. This work is licensed under a Creative Commons Attribution 4.0 License.
For more information, see https://creativecommons.org/licenses/by/4.0/

performance in Ce^{3+}-doped garnets. According to first principles simulations [12], [13], V_O (oxygen vacancy), C_O (carbon occupying oxygen site), and V_{Al} (aluminum vacancy) are the most probable among the isolated defects in as-grown crystals under reducing conditions of CO-containing atmosphere. However, the lowest formation energies are obtained for the C_O–V_{Al4} and C_i–Y_{Al} complex defects (V_{Al4} is an aluminum vacancy in a tetrahedral site, and Y_{Al} is the yttrium occupying Al sites). These defects in positive oxidation states may trap electrons, thus forming different types of color centers. The situation completely changes after annealing in air. The lowest formation energies are obtained for C_{Al}–V_O, C_O–V_{Al}, and C_i–V_{Al6} defects stabilized in negative oxidation states, which do not capture electrons and eventually do not form color centers. This presumably causes irreversible discoloration of C-doped garnets after thermal annealing [14] and a good radiation hardness (in other words, weak deterioration of transmission) under high doses of gamma-rays and high-energy protons [15]. Furthermore, according to the best of authors' knowledge, there were few systematical studies of the impact of divalent cations on scintillation and optical performance of Ce-doped garnets. One may note the work by Kamada et al. [16] where among the Mg, Ca, Sr, and Ba codoped LuAG:Ce single crystals, the fastest decay of 44–45 ns and the light yield of up to 21 300 phot/MeV were achieved in Mg- and Ca-doped samples.

This work addresses triple codoping of YAG:Ce,C with divalent cations aiming to reduce the scintillation decay time while keeping a high enough light yield, targeting the requirements to scintillators for upcoming LHCb collider experiment [8]. Therefore, we have chosen Mg^{2+}, Ca^{2+}, Sr^{2+}, and Ba^{2+} divalent cations and studied the optical and scintillation performance of YAG:Ce,C crystals codoped with these divalent ions.

II. Experiment

A. Crystal Growth and Sample Fabrication

Crystals were grown by the Czochralski method using induction heating furnace "Oxide" (Apollo Crystals, Kyiv, Ukraine). The growth process was carried out using tungsten crucibles, carbon insulation in Ar + CO atmosphere. More details can be found elsewhere [17]. The starting components in the form of Y_2O_3, Al_2O_3, CeO_2, CaO, MgO, $SrCO_3$, and $BaCO_3$ with the purity of not less than 4 N were mixed at the stoichiometric ratio and melted in W crucibles of 50 × 50 mm size. The crystals with a diameter of 10–15 mm and a cylinder height of 60–70 mm were pulled from melt with a rate of 1–2 mm/h and a rotation rate of 10 r/min with automated diameter control by a weight sensor. The samples of 5 × 5 × 2 mm and 5 × 5 × 1 mm dimensions were cut and polished for tests of optical and scintillation properties. The nominal Ce content in melt was 0.3 at.% with respect to Y, and the contents of Sr, Ba, Mg, and Ca were the same. Additionally, Ce and Ca contents in YAG:Ce,Ca were varied to optimize the Ce/Ca ratio. Then, the samples were annealed in air at 1250 °C for 24 h to reveal the role of thermal annealing on optical and scintillation parameters.

B. Characterization

The absorption spectra were registered using a Jasco 760 UV-Vis spectrometer in the 200–1100-nm range. Measurements of photoluminescence parameters were carried out in reflectance mode using a combined fluorescent lifetime and steady-state spectrometer FLS 920 (Edinburgh Instruments, Livingston, U.K.) equipped with a Xe 450-W lamp for steady-state measurements and hydrogen filled nF 900-ns flashlamp (optical pulse duration is 1.0–1.6 ns, and pulse repetition rate is 40 kHz) for time-correlated single-photon counting measurements. The CL spectra were registered using a SEM JEOL JSM-820 electron microscope equipped with a Stellar Net spectrometer and TE-cooled charge-coupled device (CCD) detector working in the 200–925-nm range.

At the first stage, scintillation light yield and scintillation decay kinetic were performed using the setup consisting of a Hamamatsu H6521 photomultiplier, homemade multichannel analyzer working with the shaping time of 12 μs, and a Tektronix TDS3052 digital oscilloscope under excitation by α-particles of ^{239}Pu (5.15 MeV) source.

As the measurements under α-particles reflect the state of just the sample surface of 12–15 μm thick, additional scintillation decay measurements were performed at ISMA NAS of Ukraine Kharkiv, Ukraine, under γ-radiation (^{137}Cs, 662 keV). Signal from Hamamatsu R6231 photo multiplier tube (PMT) anode was transferred to the input of Rigol DS6064 19 oscilloscope.

The absolute light yield was determined by comparing the peak position at pulse height spectra of our crystals with the BGO reference. The 5 × 5 mm surfaces of the crystals were polished, and the samples were covered with Teflon reflectors during measurements to improve light collection. The measurements were recorded using a pulse processing chain consisting of a R1307 PMT (Hamamatsu, Japan), a charge-sensitive preamplifier BUS 2-94 (Tenzor, Moscow, Russia), a custom-shaping amplifier, and a multichannel analyzer AMA-03F (Tenzor, 25 Russia). ^{137}Cs (662 keV) was used as a gamma-ray source. We used a reference sample with a light yield of 8600 phot/MeV produced in the Institute for Scintillation Materials NAS of Ukraine, Kharkiv. The quantum efficiencies of 0.1867 (BGO) and 0.1158 (YAG:Ce,C) were taken in the calculations based on the luminescence spectra of the crystals and the PMT quantum efficiency [18].

Scintillation decay time spectra were measured with Hamamatsu R6231 PMT excited with 662-keV γ-rays from ^{137}Cs source. Signal from PMT anode was fed to the input of Rigol DS6064 19 oscilloscope. Scintillation decay was approximated by the sum of two to three exponentials (the following equation):

$$I(t) = \sum A_i \exp\left[-\frac{t}{\tau_i}\right], \quad i = 1-3. \tag{1}$$

Contribution of the components (%) was calculated by the following equation:

$$\frac{A_i \tau_i}{A_1\tau_1 + A_2\tau_2 + A_3\tau_3} \cdot 100\%, \quad i = 1-3. \tag{2}$$

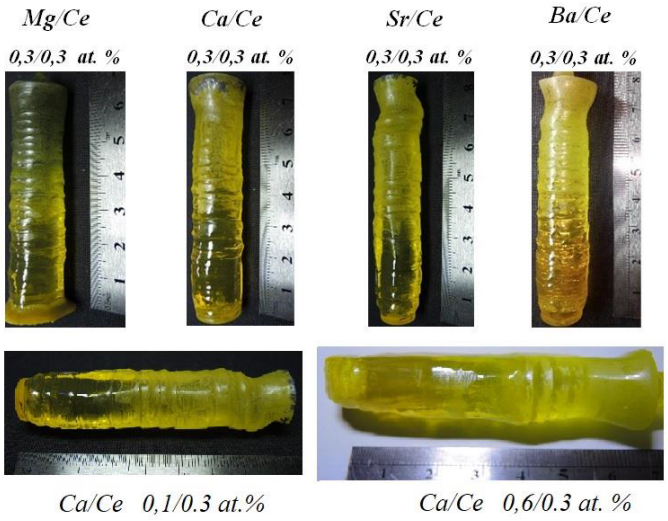

Fig. 1. As-grown YAG:Ce,C,A^{2+} crystals obtained in this work. The percentages of dopants are indicated in the legends.

Thermostimulated luminescence (TSL) glow curves were recorded using TL-reader (produced by IP PAN, Warsaw, Poland). The samples were irradiated with X-ray photons with a dose of 2 Gy produced at 6-MV accelerating voltage. For this purpose, we used the Clinac 2300C/D linear accelerator from Varian Medical System (VMS, Palo Alto, CA, USA) located in the Oncology Center, Bydgoszcz, Poland. Prior to the irradiation, samples were preheated up to 450 °C. All the measurements except TSL were performed at room temperature (25 °C).

III. Results and Discussion

A. Optical Properties of YAG:Ce,C,A^{2+} Crystals

The photographs of crystals with different codopants obtained by the Czochralski method are presented in Fig. 1. The as-grown crystals were transparent with a gray-brownish tint. The boules did not contain visible inclusions in the bulk except for the lowest part grown before the cutoff from the melt. Upper parts of the crystal lateral surfaces were etched due to the interaction with the growth atmosphere (see [17] for the details).

In Mg^{2+}- and Ca^{2+}-containing crystals, the absorption bands at 340, 458 nm related to 4f–5d transitions in Ce^{3+} weaken (Mg^{2+}) or disappear (Ca^{2+}) after the annealing with a simultaneous increase in UV absorption below 350 nm attributed to Ce^{4+}–O^{2-} charge transfer related band (Fig. 2). It is interesting that there are no manifestations of Ce^{3+} in YAG:Ce,C,Ca^{2+} absorption spectra indicating that the quantity of cerium in the trivalent state is negligibly small in the annealed samples. Previously, we observed this phenomenon in YAG:Ce,Mg single crystalline fibers obtained by the micropotential difference (PD) method [19]. At the same time, the annealing does not affect the intensity of the Ce^{3+} bands in Sr^{2+}- and Ba^{2+}-codoped samples. Presuming the 458-nm peak intensity corresponds to Ce^{3+} concentration and no Ce^{4+} in crystals grown under the reducing conditions, a negligible concentration of Ce^{3+} remains in YAG:Ce,Ca approximately half of Ce^{3+} that remains in YAG:Ce,C,Mg^{2+} and no valency change is observed in Ba^{2+}-and Sr^{2+}-codoped YAG:Ce,C.

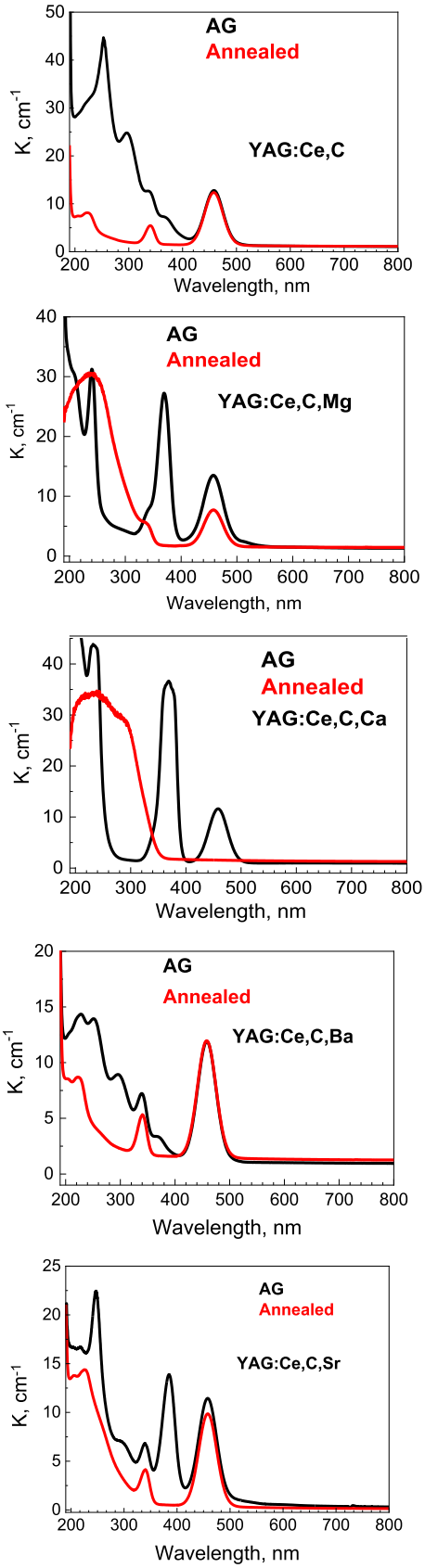

Fig. 2. Optical transmission spectra of YAG:Ce,C,A^{2+} before/after the annealing.

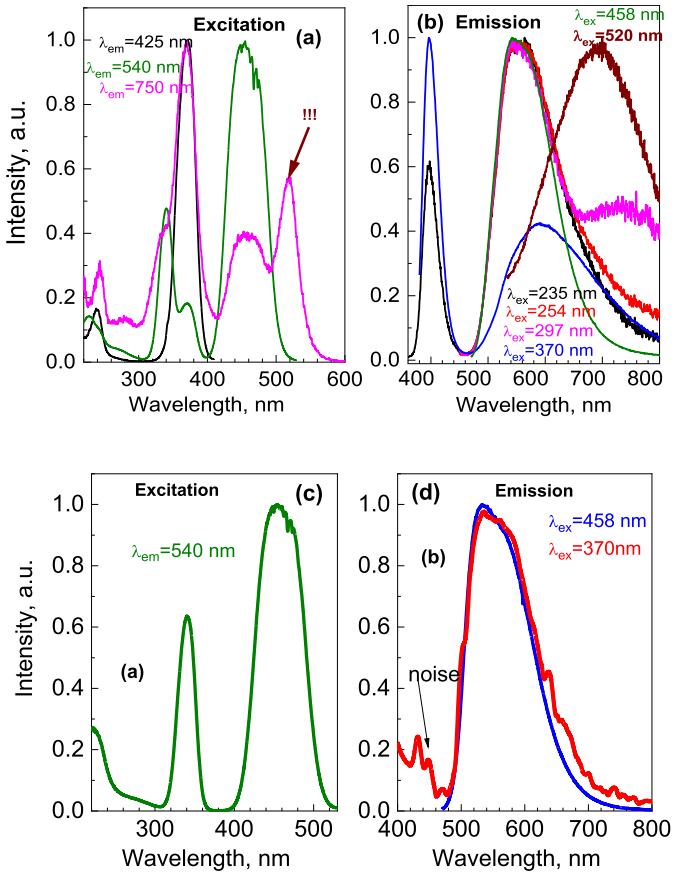

Fig. 3. Excitation and emission spectra of YAG:Ce,C,Mg^{2+}: (a) and (b) before and (c) and (d) after the annealing.

Meanwhile, the sharp absorption bands around 370 nm attributed to F^{+}-centers in garnets [20] and 230 nm attributed to Ce^{3+} absorption [10], [21] are suppressed in the annealed YAG:Ce,C codoped with Ca^{2+}, Mg^{2+}, and Sr^{2+}, whereas UV-absorption related to Ce^{4+}–O^{2-}charge transfer complexes remarkably enhances in the annealed crystals except YAG:Ce,C,Sr^{2+} crystal. Summarizing, postgrowth annealing suppresses color center formation at Ca^{2+}-, Mg^{2+}-, or Sr^{2+}-doping, while Ca^{2+}- and Mg^{2+}-doping also promotes the formation of tetravalent Ce^{4+} ions. The decrease of color center related absorption in UV is observed with Ba^{2+} doping. From the point of compensation of lacking positive charge per one Y^{3+} cation in the as-grown samples substituted by Ca^{2+} and Mg^{2+}, anionic vacancies may form (one O^{2-} vacancy for two $(Ca/Mg)^{2+}$), which can capture electrons and form F^{+}-centers. Therefore, an intense band at 370 nm in as-grown crystals in this case serves as an indirect indicator of incorporation of divalent codopants. Its intensity is small in the case of Ba^{2+} codoping because this cation probably does not enter the lattice in sufficient quantity. The different behavior of the Ba^{2+}-codoped sample may be attributed to a very large ionic radius of Ba^{2+}, thus leading to the formation of some additional defects at Y^{3+}/Ba^{2+} substitution.

All decay curves of Ce^{3+} luminescence in divalent codoped crystal under excitation in the UV-range (458 nm) (not shown) are well fit by single-exponential function. The decay times in all the crystals under study are within 56–63 ns. No clear trends in the change of decay profiles before/after annealing were observed.

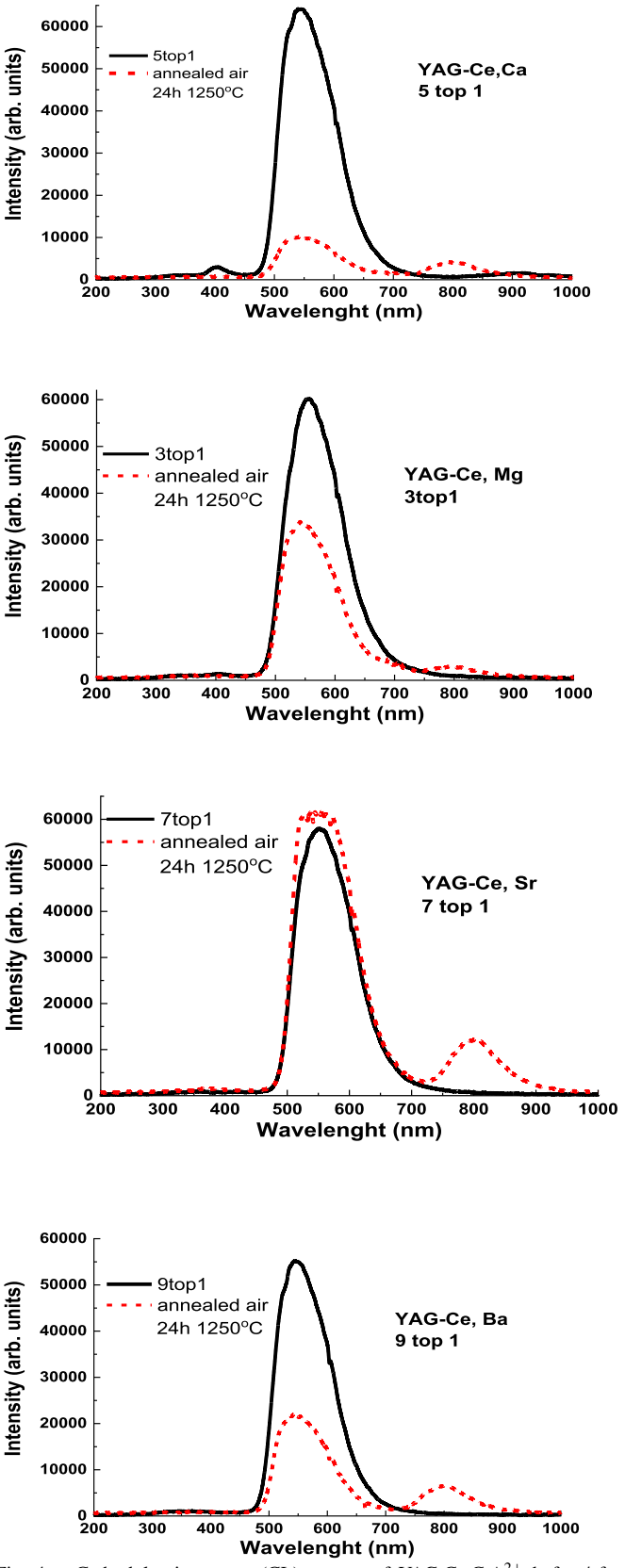

Fig. 4. Cathodoluminescence (CL) spectra of YAG:Ce,C,A^{2+} before/after the annealing.

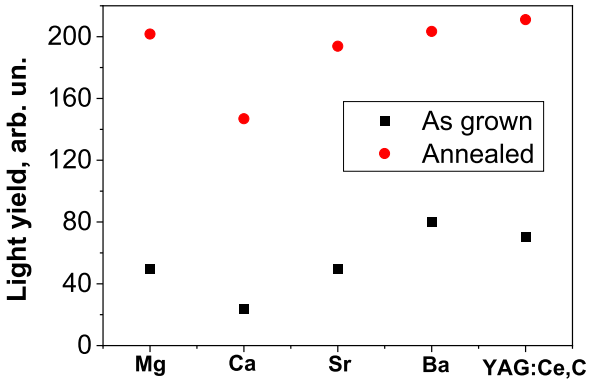

Fig. 5. Relative light yield (without the correction for PMT sensitivity) of YAG:Ce,C,A^{2+} before/after the annealing.

Meanwhile, some interesting features are revealed in the UV–visible excitation and emission spectra. Let us illustrate them on the example of Mg^{2+}-codoped crystals (Fig. 3). While the excitation and emission spectra in all the codoped crystals after the annealing are identical with the Ce^{3+} excitation peaks at 220, 340, and 460 nm and emission peak at 455 nm, there are some specific features on the spectra of as-grown crystals. Along with the mentioned Ce^{3+}-related peaks, there is a broad emission peaked around 750 mm with a complex excitation spectrum. The latter is excited in both Ce^{3+} excitation peaks, and the 370-nm peak associated with F^{+}-centers [22] and the 520 peak of an unknown nature. Similar emission was registered by us in YAG:C without codoping with divalent cations [10] and related to carbon-related defects/or aggregates of charged oxygen vacancies. However, all these bands disappear after the annealing in air. At the same time, an impact of impurities such as Fe and Cr, which may emit in a reduced state, e.g., Fe(II) or Cr(II) and their luminescence disappears in the trivalent state after annealing in air should not be ruled out.

B. Scintillation Properties of YAG:Ce,C,A^{2+} Crystals

A decrease in the Ce^{3+} peak intensity at 550 nm in the CL spectra (Fig. 4) after the annealing in all the samples except Sr^{2+}-doped one, in general, corresponds to the weakening of Ce^{3+} absorption bands in Fig. 2, confirming the Ce^{3+} transfer into the tetravalent state under the oxidizing conditions. Note the weakest intensity is registered in YAG:Ce,C,Ca where the Ce^{3+} absorption is negligible (see Fig. 2). Moreover, all the spectra contain a very weak band in UV-range related to emission centers associated with antisite defects [20] and a wide band around 800 nm. The latter may be attributed to Fe^{3+} emission [23] rising after the annealing or aggregates of charged oxygen vacancies.

Switching to light yield, in Mg^{2+}-, Sr^{2+}-, and Ba^{2+}-doped crystals, it is similar to that in YAG:Ce,C both before and after the annealing [10], while it is remarkably lower only in YAG:Ce,Ca^{2+} where a concentration of Ce^{3+} centers is very low (Fig. 5). This supports the suggestion by Nikl et al. [3] regarding the positive impact of partial (but incomplete) transfer of Ce^{3+} ions to the tetravalent state on scintillation performance. It is interesting to note the sharp enhancement of light yield at simultaneous reducing of the CL intensity after the annealing in all the samples, expect the Sr^{2+}-codoped crystal where the CL peak intensity does not change remarkably.

TABLE I

SCINTILLATION DECAY TIMES (NS) AND CONTRIBUTIONS OF DECAY COMPONENTS (%) IN YAG:CE,C,A^{2+} UNDER IRRADIATION BY γ-RAYS (^{137}CS, 662 KEV)

	As-grown			Annealed		
	τ1	τ2	τ3	τ1	τ2	τ3
Mg	58 (14%)	230 (55%)	819 (31%)	78 (37%)	368 (52%)	1260 (11%)
Ca	40 (19%)	131 (43%)	805 (38%)	55 (77%)	282 (23%)	
Sr	74 (34%)	286 (49%)	1698 (17%)	73 (33%)	327 (37%)	25862 (30%)
Ba	118 (49%)	465 (51%)		111 (30%)	367 (48%)	6668 (22%)
YAG: Ce,C				101 (19%)	359 (60%)	2260 (21%)

TABLE II

SCINTILLATION DECAY TIMES (NS) AND CONTRIBUTIONS OF DECAY COMPONENTS (%) IN YAG:CE,C,CA^{2+} CRYSTALS WITH VARIED CE/CA^{2+} RATIO

	As-grown			Annealed		
	τ1	τ2	τ3	τ1	τ2	τ3
0,1%Ca, 0,3%Ce	71 (22%)	275 (50%)	1345 (28%)	74 (52%)	362 (48%)	-
0,3%Ca, 0,3%Ce	40 (19%)	131 (43%)	805 (38%)	55 (77%)	282 (23%)	-
0,6%Ca, 0,3%Ce	46 (13%)	158 (47%)	992 (40%)	59 (75%)	270 (25%)	-
1%Ca, 1%Ce	69 (72%)	458 (28%)	-	55 (96%)	347 (4%)	-

Scintillation decay accelerates after the annealing in all the samples (Fig. 6), most remarkably in YAG:Ce,Ca. The decay times fit with two or three exponential functions are quantitatively compared in Table I. The Ca^{2+}- and Mg^{2+}-codoping is the most promising for fast timing applications. However, the decrease in decay times in YAG:Ce,C,Ca is achieved at the expense of light yield, in agreement with the numerous data on C-free garnets [3], [4], [5], [6]. As the main decay time of 55 ns in YAG:Ce,C,Mg^{2+} is too slow for the desired application, tuning the Ce^{3+} and codopant concentrations or combined codoping with two divalent cations may be useful for further acceleration of scintillation decay.

The main TSL peaks around 150 °C and 250 °C–300 °C are observed in all as-grown crystals with different intensity ratios between them (Fig. 7). There is a common tendency of

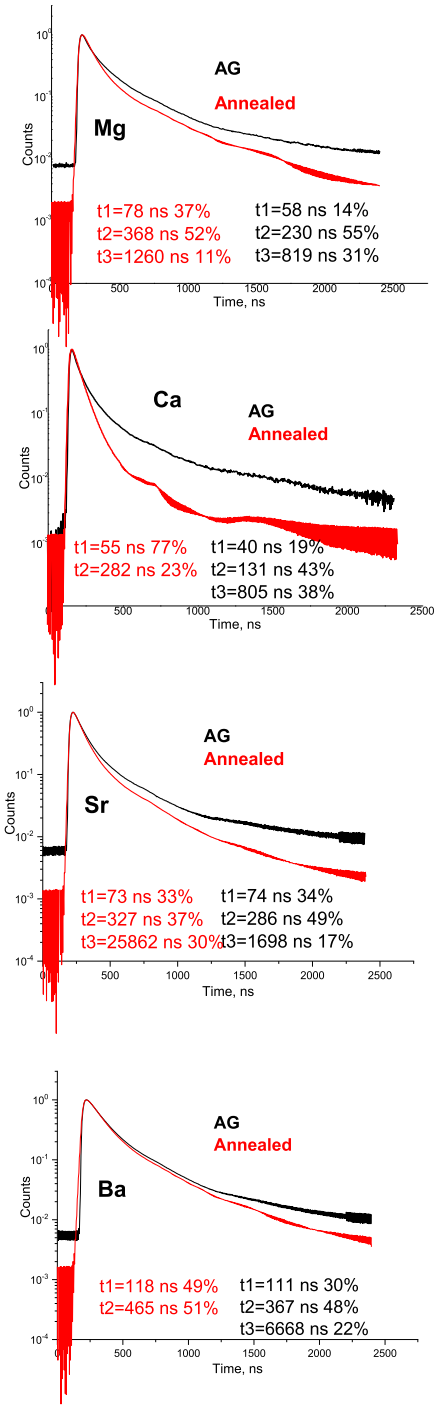

Fig. 6. Scintillation decay of YAG:Ce,C,A^{2+} under γ-ray excitation (^{137}Cs, 662 keV) before/after the annealing.

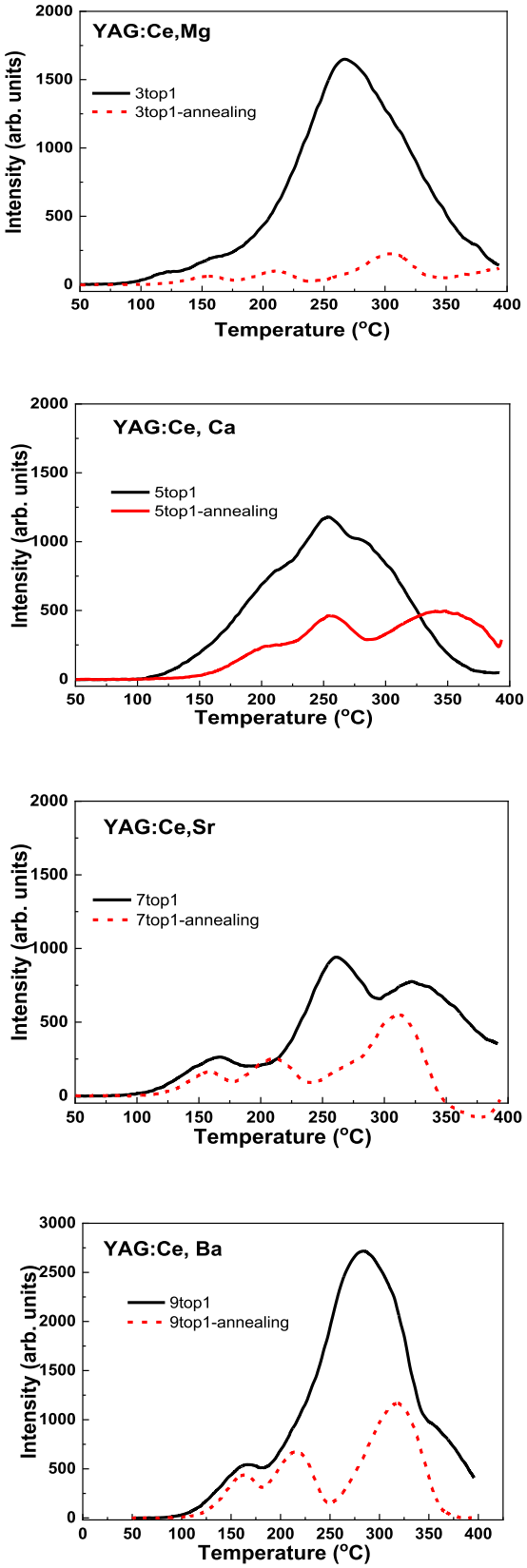

Fig. 7. TSL curves of YAG:Ce,C,A^{2+} before/after the annealing.

decreasing the TSL intensity after the thermal annealing, certifying a decrease in defect concentration and carrier trapping. The main remaining peaks are at 150 °C, 200 °C, and 310 °C (YAG:Ce,C,Mg), 220 °C and 325 °C (YAG:Ce,C,Ca), 150 °C, 200 °C, and 310 °C (YAG:Ce,C,Sr), and 150 °C, 200 °C, and 315 °C (YAG:Ce,Ba).

The most striking difference between the samples is weakly manifested 150 °C peak and the shift of >300 °C peak to higher temperatures in the Ca^{2+}-codoped sample. In general, the structure of TSL curves is similar to that reported for oxygen-deficient YAG:C [24] and YAG:Ce in the form of single crystals and optical ceramics [25].

There is a tendency to a higher intensity of the high-temperature glow above 300 °C in the samples studied

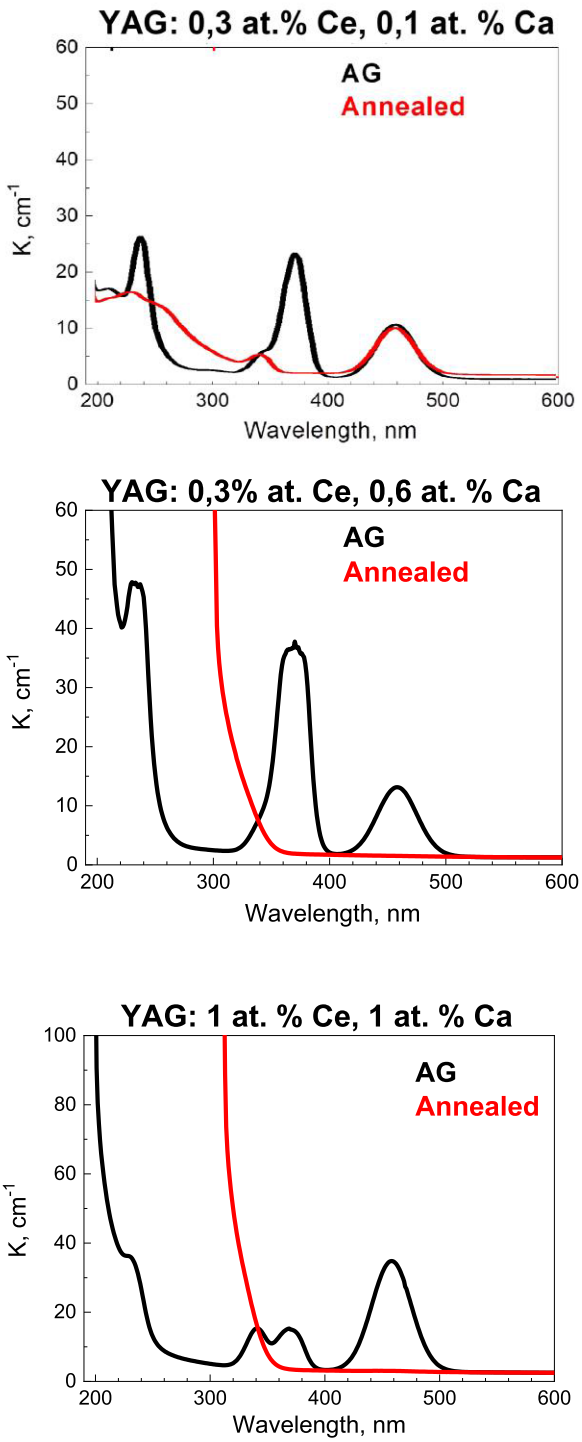

Fig. 8. Absorption spectra of YAG:Ce,C,Ca^{2+} crystals with different Ce and Ca concentrations.

in this work, which may point at deep traps associated with carbon-related defects. However, a detailed interpretation of the peak nature is complicated due to the large amount of possible defect types created at carbon doping.

C. Tuning the Codopant Concentration in YAG:Ce,C,Ca^{2+}

As the shortest decay times were registered in the Ca^{2+}-codoped sample, the crystals with the codopant content from

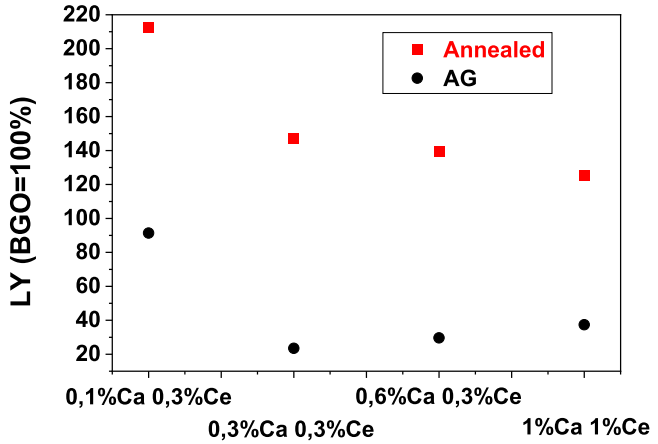

Fig. 9. Light yield (without a correction for PMT sensitivity) of YAG:Ce,C,Ca^{2+} crystals with different Ce/Ca ratios. The 100% corresponds to the BGO scintillator with a light yield of 8600 phot/MeV.

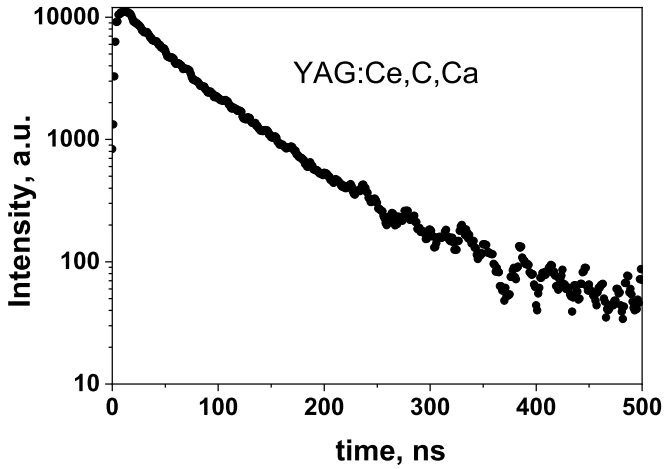

Fig. 10. Scintillation decay curve of YAG:1%Ce,C,1%Ca^{2+} crystal under γ-rays.

0.1 to 1 at.% and Ce content from 0.3 to 1 at.% were grown, thus tuning the Ce/Ca ratio.

Expectedly, the Ce^{3+} absorption around 450 nm is completely suppressed after the annealing at the Ce/Ca ratios below unity (Fig. 8), and the light yield monotonously decreases with Ca^{2+} concentration (Fig. 9). The main decay constant of around 55 ns has not decreased, but in the 1%Ce, 1%Ca sample, its contribution reaches 96%, with practically no slow components (Fig. 10, Table II). Accounting for the light collection coefficient of an R1307 PMT indicated in Section II, the light yield of this sample is approximately 17 500 phot/MeV. Therefore, despite the remarkable decrease in light yield, the main decay time does not decrease below the 55–59-ns range corresponding to intrinsic radiation lifetime of Ce^{3+} in garnets [26]. The tradeoff between light yield and decay time was not resolved by the sole Ca^{2+} codoping, and the works on codoping are on the way.

IV. Conclusion

Effects of codoping with divalent ions on absorption, luminescence, and scintillation properties were verified with

M^{2+} = Ba^{2+}, Ca^{2+}, Mg^{2+}, Sr^{2+}. Ba^{2+} ions due to its large ionic radius poorly entered the lattice and barely affected the optical and scintillation performance YAG:Ce,C,Ba^{2+} crystals. We have also found that Ca^{2+}, Mg^{2+}, and Sr^{2+} codopants promoted the formation of tetravalent Ce^{4+} ions and acceleration of scintillation decay by the mechanisms priorly described for A^{2+}-doped garnets (A = Ca, Mg) and orthosilicates. However, the main scintillation decay time did not decrease in all the crystals under study below the Ce^{3+} intrinsic lifetime of ca. 55 in garnet hosts. Furthermore, the contribution of long components of scintillation decay, related to intrinsic lattice defects, was reduced in YAG:Ce,C,Ca crystals to 4% by tuning the Ce/Ca ratio with retaining the light yield of 17 500 phot/MeV, and further work should be focused on the combination of codoping with different divalent cations.

ACKNOWLEDGMENT

This work was made in the frame of Horizon Europe ERA Widening Project no. 101078960 "TWISMA" and International Research Project "ScintLab" of CNRS, Paris, France.

REFERENCES

[1] M. S. Alekhin, D. A. Biner, K. W. Kramer, and P. Dorenbos, "Improvement of LaBr3:5%Ce scintillation properties by Li^{+}, Na^{+}, Mg^{2+}, Ca^{2+}, Sr^{2+}, and Ba^{2+} co-doping," *J. Appl. Phys.*, vol. 113, 2013, Art. no. 224904.

[2] S. Blahuta, A. Bessiere, B. Viana, P. Dorenbos, and V. Ouspenski, "Evidence and consequences of Ce^{4+} in LYSO:Ce, Ca and LYSO:Ce,Mg single crystals for medical imaging applications," *IEEE Trans. Nucl. Sci.*, vol. 60, no. 4, pp. 3134–3141, Aug. 2013, doi: 10.1109/TNS.2013.2269700.

[3] M. Nikl et al., "Defect engineering in Ce-doped aluminum garnet single crystal scintillators," *Cryst. Growth Des.*, vol. 14, no. 9, pp. 4827–4833, Sep. 2014.

[4] P. Prusa et al., "Tailoring and optimization of LuAG:Ce epitaxial film scintillation properties by Mg co-doping," *Crystal Growth Des.*, vol. 18, no. 9, pp. 4998–5007, Sep. 2018.

[5] A. Belsky et al., "Mechanisms of luminescence decay in YAG-Ce,Mg fibers excited by γ- and X-rays," *Opt. Mater.*, vol. 92, pp. 341–346, Jun. 2019.

[6] W. Ma et al., "On fast LuAG:Ce scintillation ceramics with Ca^{2+} co-dopants," *J. Amer. Ceram. Soc.*, vol. 104, no. 2, pp. 966–973, 2021.

[7] M. Kucera, M. Rathaiah, M. Nikl, A. Beitlerova, O. Lalinsky, "Scintillation properties of $YAlO_3$:Ce perovskite co-doped by Mg^{2+} ions," *Opt. Mater.*, vol. 132, Oct. 2022, Art. no. 112779, doi: 10.1016/j.optmat.2022.112779.

[8] L. Martinazzoli et al., "Compositional engineering of multicomponent garnet scintillators: Towards an ultra-accelerated scintillation response," *Mater. Adv.*, vol. 3, no. 17, pp. 6842–6852, 2022.

[9] V. Babin, P. Herman, M. Kucera, M. Nikl, and S. Zazubovich, "Effect of Mg^{2+} co-doping on the photo- and thermally stimulated luminescence of the $(Lu,Gd)_3(Ga,Al)_5O_{12}$:Ce epitaxial films," *J. Lumin.*, vol. 215, Nov. 2019, Art. no. 116608.

[10] O. Sidletskiy et al., "Impact of carbon co-doping on the optical and scintillation properties of a YAG:Ce scintillator," *Crystal Growth Des.*, vol. 21, no. 5, pp. 3063–3070, May 2021.

[11] D. Kofanov et al., "LuAG:Ce and LuYAG:Ce scintillation crystals grown under reducing conditions from W crucibles," *Opt. Mater.*, vol. 134, Dec. 2022, Art. no. 113176.

[12] J. Zhu, O. Sidletskiy, Y. Boyaryntseva, and B. Grynyov, "Structure and role of carbon-related defects in yttrium aluminum garnet," *Opt. Mater.*, vol. 111, Jan. 2021, Art. no. 110561.

[13] L. Jia, J. Zhu, Y. Boyaryntseva, I. Gerasymov, B. Grynyov, and O. Sidletskiy, "Effect of carbon doping on F-type defects in YAG and YAG:Ce crystals," *Phys. Status Solidi (B)*, vol. 258, no. 12, Dec. 2021, Art. no. 2100325.

[14] S. Tkachenko et al., "Control of optical properties of YAG crystals by thermal annealing," *J. Cryst. Growth*, vol. 483, pp. 195–199, Feb. 2018.

[15] V. Dormenev et al., "Radiation tolerant YAG:Ce scintillation crystals grown under reducing Ar+CO atmosphere," *Nucl. Instrum. Methods Phys. Res. Sect. A, Accel., Spectrometers, Detectors Associated Equip.*, vol. 1015, Nov. 2021, Art. no. 165764.

[16] K. Kamada et al., "Co-doping effects on luminescence and scintillation properties of Ce doped $Lu_3Al_5O_{12}$ scintillator," *Nucl. Instrum. Methods Phys. Res. Sect. A, Accel., Spectrometers, Detectors Associated Equip.*, vol. 782, pp. 9–12, May 2015.

[17] O. Sidletskiy et al., "Garnet crystal growth in non-precious metal crucibles," in *Engineering of Scintillation Materials and Radiation Technologies*, vol. 227, M. Korzhik and A. Gektin, Eds. Cham, Switzerland: Springer, 2019, pp. 83–95.

[18] O. Sidletskiy et al., "Drastic scintillation yield enhancement of YAG:Ce with carbon doping," *Phys. Status Solidi (A)*, vol. 215, no. 14, Jul. 2018, Art. no. 1800122.

[19] V. Kononets et al., "Development of YAG:Ce,Mg and YAGG:Ce scintillation fibers," in *Engineering of Scintillation Materials and Radiation Technologies*, M. Korzhik and A. Gektin, Eds. Cham, Switzerland: Springer, 2017, pp. 114–128.

[20] Y. Zorenko et al., "Exciton and antisite defect-related luminescence in $Lu_3Al_5O_{12}$ and $Y_3Al_5O_{12}$ garnets," *Phys. Status Solidi (B)*, vol. 244, no. 6, pp. 2180–2189, Jun. 2007.

[21] P. A. Tanner, L. Fu, L. Ning, B.-M. Cheng, and M. G. Brik, "Soft synthesis and vacuum ultraviolet spectra of YAG:Ce^{3+} nanocrystals: Reassignment of Ce^{3+} energy levels," *J. Phys., Condens. Matter*, vol. 19, no. 21, May 2007, Art. no. 216213.

[22] A. Pujats and M. Springis, "The F-type centres in YAG crystals," *Radiat. Effects Defects Solids*, vol. 155, pp. 65–67, Nov. 2021.

[23] K. Pressel, G. Bohnert, A. Dörnen, and K. Thonke, "Optical study of the Fe^{3+}-related emission at 0.5 eV in InP:Fe," *MRS Proc.*, vol. 262, pp. 301–306, 1992.

[24] Y. Zhydachevskyy et al., "Photoluminescence and thermoluminescence of the oxygen-deficient YAG, YAP, and YAM phosphors," *Acta Phys. Polonica A*, vol. 133, no. 4, pp. 977–980, Apr. 2018.

[25] E. Mihóková et al., "Luminescence and scintillation properties of YAG:Ce single crystal and optical ceramics," *J. Lumin.*, vol. 126, no. 1, pp. 77–80, Sep. 2007.

[26] P. Dorenbos, "Electronic structure and optical properties of the lanthanide activated $RE_3(Al_{1-x}Ga_x)_5O_{12}$ (RE=Gd, Y, Lu) garnet compounds," *J. Lumin.*, vol. 134, pp. 310–318, Feb. 2013.